Journal of Bio- and Tribo-Corrosion (2020) 6:126
https://doi.org/10.1007/s40735-020-00424-0

Electrochemical and Mechanical Studies of Epoxy Coatings Containing Eco-Friendly Nanocomposite Consisting of Silane Functionalized Clay–Epoxy on Mild Steel

J. Raja Beryl[1] · Joseph Raj Xavier[1]

Received: 30 March 2020 / Revised: 13 August 2020 / Accepted: 11 September 2020 / Published online: 19 September 2020

Abstract
In this study, new clay/silane/epoxy nanocomposites (CSE nanocomposite) were fabricated to enhance the corrosion resistance of epoxy resin. The surface of the clay is modified using 3-aminopropyltriethoxysilane (APTES). The functionalized clay nanoparticle was characterized by Fourier-transform infrared spectroscopy, and thermogravimetric analysis. The fabricated clay nanocomposites coated mild steel was evaluated by electrochemical impedance spectroscopy, scanning electrochemical microscopy and X-ray diffraction (XRD) studies in 3.5% NaCl solution for various days. The experiments indicated that the best epoxy coating performance was obtained by the incorporation of functionalized clay nanoparticles 4 wt% in the epoxy resin. The coated mild steel by CSE nanocomposites showed higher coating resistance ($R_c = 238{,}967\ \Omega\ cm^2$) than that of neat epoxy coating ($R_c = 129{,}532\ \Omega\ cm^2$). Mechanical properties of the coatings were also found to be improved in the presence of modified clay nanoparticle in tensile and hardness measurements. The use of nanoclays enhanced the anticorrosive behavior and physical integrity of the polymer–clay coatings under immersion tests. The surface morphology of the coated sample was analyzed by field-emission scanning electron microscopy and energy-dispersive X-ray spectroscopy. XRD analysis confirms the formation of metal complexes as the corrosion products at 40 days of immersion in 3.5% NaCl solution.

Keywords Steel · Corrosion · Protection · Coatings · Epoxy–clay nanocomposites · Silane · SECM

1 Introduction

Mild steels are widely used in fabrication of reaction vessels, building applications, petroleum refinery, and automotive industry. However, their susceptibility to corrosion has become a leading cause of either failure or unfitness for application in engineering components, thus both causing tremendous economic loss and posing a serious threat to national resources. In order to control the corrosion of metals, polymers are used as the protective coating materials. The presence of micropores in the polymer coating causes the initiation of corrosion process at the metal/coating interface. To overcome these difficulties, nanoparticles are incorporated into the polymers to produce nanocomposite coatings. However, the addition of functionalized nanoparticles in the polymers enhances the coating resistance and mechanical properties of the resultant nanocomposite coatings.

Halloysite is a clay mineral with the empirical formula $Al_2Si_2O_5(OH)_4$ [1]. The halloysites are composed of Al, O, and Si with the atomic proportion of 1:4:6:1 [2]. The aluminosilicate clay nanotubes have an Al:Si ratio of 1:1. Halloysite nano-clay is an unusual and rare natural nanotubular material. It can be widely used as an environmentally friendly clay material. Halloysite has a good biocompatibility [3], high specific surface area and a strong adsorption. However, halloysites showed a weak affinity because of the weak intermolecular forces, such as van der Waals forces and hydrogen bonding. Surface modification of clay is very desirable to improve its performance. For example, modified clay can be used as nanofillers in composite polymers to enhance mechanical strength [4]. It was found that the addition of halloysite nano-clay in an epoxy resin showed significant improvement in the anticorrosive and barrier properties of the coating compared with the epoxy coating.

✉ Joseph Raj Xavier
drjosephrajxavier@gmail.com

[1] Department of Chemistry, Vel Tech Rangarajan Dr. Sagunthala R&D Institute of Science and Technology, Avadi, Chennai, Tamil Nadu 600 062, India

Silane has been used as modifiers for nano-clay. The silane coupling agents have a general structure of $(XO)_3SiY$, where XO is a hydrolyzable alkoxy group, which can be methoxy ($–OCH_3$) or ethoxy ($–OC_2H_5$) and Y is an organo functional group. The formation of silane films is based on the condensation reactions between silanols (Si–OH), hydrolysis product of alkoxy group and the metal hydroxide (Me-OH). The organo functional silane films deposited on the metal are usually hydrophobic. They can act as a physical barrier against water. Grafted silane coupling agent onto the surface is the most common chemical modification method for halloysite clay. The silane coupling agent can react with the halloysite clay through physical or chemical bonding. 3-aminopropyltriethoxysilane (APTES) coupling agents lead to better compatibility and uniform dispersion in the mild steel-based silane coating. In addition, the silane films can also act as adhesion promoters between metal substrate and organic coatings. Polymer–clay nanocomposites have attracted a lot of attention. Incorporation of a small amount (1–5 wt%) of clay into organic polymers leads to significant improvements in mechanical performance [5–9], thermal stability [10–15], barrier properties, and properties such as dimensional stability, reduced gas permeability, optical clarity, and flame retardancy of organic coatings [16–19]. The halloysite clay nanoparticles improved the quality of the cured epoxy coating, reduced the porosity of the coating matrix and prolonged the diffusion path as well as improved the adhesion properties to the underlying substrate compared to other coatings. Among polymer layered silicate (clay) nanocomposites, epoxy-based systems has been reported in detail, due to the ease of processing as well as its versatile applications in various fields. The structure and properties of epoxy clay nanocomposites are influenced by the curing agents, clay modifier and processing method. An impressive progress has been reported during the last few years regarding the preparation and the use of polymer–clay nanocomposites for corrosion protection. These materials offer a number of advantages, such as excellent mechanical and thermal stability, improved anticorrosion protection, and wide accessibility of clay compared to other coating systems [20–22].

In the present research, halloysite nano-clay was modified by 3-aminopropyltriethoxysilane (APTES) and incorporated into an epoxy matrix using direct mixing under an ultrasonic Homogenizer. Thermogravimetric analysis (TGA) has been used to evaluate the thermal stability of polymer and their nanocomposites. The protection capabilities of epoxy-APTES/clay nanocomposite coatings were examined. Anticorrosion properties of the coatings were investigated using electrochemical impedance spectroscopy (EIS) [23] and scanning electrochemical microscopy (SECM) [24, 25]. Scanning electron microscopy (SEM)/energy dispersive X-ray analysis (EDX) was used to characterize the coating structure and the presence of elements both in the steel/epoxy coating interface and the modifier coating. Mechanical properties were examined by adhesion pull off test, tensile test, and hardness test.

2 Experimental Details

2.1 Materials

The halloysite nano-clay used in this study was obtained from Sigma-Aldrich. The diglycidyl ether of bisphenol A (DGEBA) epoxy resin and the amine containing hardener (Epikure F205) were purchased from Sigma-Aldrich. 3-aminopropyltriethoxysilane and acetone (98.5%) purchased from Sigma Aldrich, were used as received. Table 1 presents the chemical specifications and formulae for the materials used in the epoxy-APTES/clay nanocomposite preparation. Samples of mild steel sheets (20 × 10 × 3 mm) were used as the substrate. Its composition in percentage weight was C = 0.05, Mn = 0.013, Si = 0.012, P = 0.10, Al = 0.1, S = 0.012 and Fe = 99.6. The samples were abraded with grid sizes from 200 to 1200 grades and cleaned with ethanol.

2.2 Surface Modification of Clay Nanoparticles

An equimolar proportion of halloysite clay (4.40 g) and APTES (3.32 g) were kept in a vacuum chamber for 1 h at 120 °C and then dispersed in 30 ml acetone via stirring at 300 rpm for 1 h at ambient temperature. Then, the

Table 1 The chemical specifications and formulae for the materials used in the epoxy-APTES/clay nanocomposite preparation

Materials	Chemical specifications	Formula	Source	Particle size
Halloysite nano-clay	White to Tan nanopowder	$Al_2Si_2O_5(OH)_4{\cdot}2H_2O$	Sigma Aldrich	30–70 nm × 1–3 µm, nanotube
Diglycidyl ether of bisphenol A epoxy resin	Colorless viscous liquid	$C_{21}H_24O_4$	Sigma Aldrich	–
Epikure F205	Colorless liquid (99%)	$C_{10}H_{22}N_2$	Sigma Aldrich	–
3-Aminopropyl-triethoxysilane	Colorless liquid (98.5%)	$H_2N(CH_2)_3Si(OC_2H_5)_3$	Sigma Aldrich	–

suspension was centrifuged (6000 rpm) and sonicated at 40 °C for 20 min. The resulting precipitate was filtered and washed with water; it was repeated for three times. APTES-modified clay was then dried at 80 °C in a vacuum oven for 2 days. The grafting of APTES on the halloysite nanoparticles was evaluated by FTIR, and TGA. FTIR spectroscopy was carried out in KBr pellet, collecting 35 scans in the 400–4000 cm^{-1} range with 4 cm^{-1} resolution. Thermogravimetric analysis (TGA) has been used to evaluate the thermal stability of polymers and their nanocomposites.

2.3 Preparation of Epoxy-Based Nanocomposites Coatings

The APTES-modified clay was incorporated into the epoxy coating at different concentration. The best corrosion protection was obtained with 4 wt% clay content. Samples were mechanically cleaned by scrubbing with a little brush and chemically cleaned using ethanol followed by acetone to be prepared for immediate application of the coating after polishing. The liquid paints (pure epoxy and epoxy resin containing APTES/clay) were applied on the polished metal samples by draw down bar. After drying (ambient temperature for 24 h), the coatings were about 40 µm thick (measured by a Minitest 600 Erichen digital meter).

2.4 Electrochemical Characterization of Coated Specimens

After exposure for 1, 10, 20 and 40 days in a corrosive environment of 3.5% NaCl solution, Impedance measurements were carried out in Autolab Potentiostat/Galvanostat, PGSTAT100 (NOVA Software). The frequency scan was carried out over a range from 100 kHz to 10 MHz and at an amplitude sinusoidal voltage of ± 10 mV [26]. A conventional three compartment glass cell was used. A platinum foil with a surface area of 1 cm^2 was used as the counter electrode, saturated calomel electrode (SCE) was used as the reference electrode, steel samples in 1 cm^2 exposed area was used as a working electrode. All impedance measurements were carried out at 25 °C, in de-aerated conditions and at the potential value of the corrosion potential (E_{corr}). Polarization curves were obtained at 0.167 mV/s sweep rate in the range of − 250 to + 250 mV (vs. SCE) from OCP. Nanocomposite coatings with 4 wt% concentrations were prepared and compared with neat epoxy coating through EIS measurements.

The scanning electrochemical microscopy (SECM) measurements were done in 3.5% NaCl solution using CHI920 (CH-Instruments, Austin, Texas, USA). SECM used a platinum microelectrode tip with a diameter of 10 µm. The Ag/AgCl was used as a reference electrode and a Pt wire was used as a counter electrode. An optically encoded inchworm piezo motor was utilized for controlling the tip movement along the x, y and z directions. The potentials of the sample and tip are controlled separately by a biopotentiostat [27]. A video microscope helps to position the microelectrode over the coated sample. The scratched coated mild steel was kept at the bottom of the cell in a horizontal position.

2.5 Characterization of Coated Specimen

The surface morphology and elemental composition of epoxy-APTES/clay nanocomposite coated mild steel were characterized by field emission scanning electron microscopy (FE-SEM) with energy dispersive X-ray (EDX) analysis (Model CARL ZEISS SUPRA 55, Germany). X-ray diffraction (XRD) was also applied to determine the degree of intercalation/exfoliation of clay nanoplatelets within the epoxy polymer. XRD measurements were performed on a Siemens D 500 (Siemens AG, Karlsruhe, Germany) type automated diffractometer, with Cu(Kα) $\lambda = 1.5418$ Å radiation, in the range 10°–70° 2θ angles and at a scan rate of 1°/min.

The mechanical properties of the samples were measured with an Instron 3344 dynamometer (Instron, Norwood, MA, USA) according to the Standard Method (ASTM D638), with a stress rate of 5 mm/min. The adhesion strength of the coatings to the substrate was carried out before and after immersion in 3.5% NaCl solution by pull-off measurements on Electronic Universal Material Testing Machine (Instron Corporation, USA). The testing was done according to ASTM D3359 standard. The tensile test was performed with the universal testing machine at a cross head speed of 10 mm/min. In tensile testing, a "dog-bone" shaped sample is placed in the grips of movable and stationary fixtures in a screw driver device, which pulls the sample until it breaks and measures applied load versus elongation of the sample. The measurement of micro hardness was carried out using HM113 Vickers hardness tester. The right angle pyramid with a square base diamond indentor angle of 136° between opposite faces compressed the composite specimen under a load of $F = 20$N for a loading time of 15 s. Six numbers of indentation were made on each sample to get the mean value of the hardness.

3 Results and Discussion

3.1 FTIR Spectroscopy

The FTIR spectra of APTES, pure halloysite clay and APTES-modified halloysite clay are shown in Fig. 1. After the modification with APTES, some dramatic changes are observed in the FTIR spectrum of the APTES-modified halloysite. The double peaks of pure APTES at 3213 cm^{-1} and 3040 cm^{-1} are due to $–NH_2$ stretching mode. The peak at

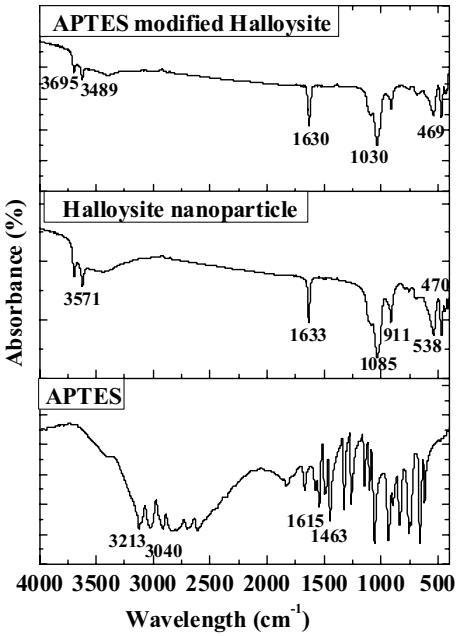

Fig. 1 FTIR spectra obtained for APTES, Halloysite nanoparticle and APTES-modified halloysite

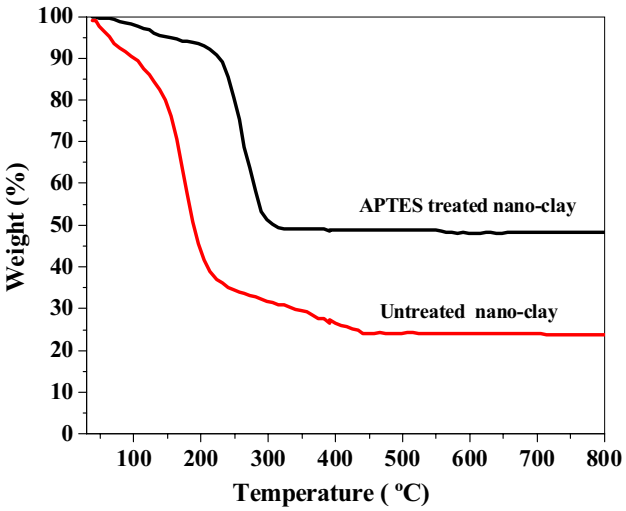

Fig. 2 TGA curves of untreated nano-clay and APTES treated nano-clay

3695 cm^{-1} for APTES-modified halloysite is due to free OH groups. The band at 3489 cm^{-1} is attributed to the stretching and bending modes of adsorbed water molecules. The peak at 469 cm^{-1} corresponds to the bending vibration of Si–O–Si. It is evident that N–H stretching has shifted from 3213 cm^{-1} to 3695 cm^{-1}. The C=C bond has shifted from 1615 cm^{-1} to 1630 cm^{-1}. The C=O stretching bond shifted from halloysite 1085 cm^{-1} to APTES halloysite 1030 cm^{-1}. The peaks, appearing in 1085, 1030, 538 cm^{-1} are associated to in plane and out of the plane of the CH chains. All these changes revealed that the halloysite nano-clay had been successfully modified by the addition of APTES.

3.2 Thermogravimetric Analysis (TGA)

Figure 2 shows the TGA thermograms of untreated nano-clay, and APTES-treated nano-clay. Thermal analysis of treated and untreated nano-clay showed a three-step weight loss, the first step (I) from 30 to 180 °C the total mass loss of ~ 21.29% occurs for untreated nano-clay and in APTES treated nano-clay total mass loss of ~ 5.10% occurs. The weight loss at this temperature corresponds to the elimination of physisorbed water molecules and nitrate ions present in untreated nano-clay surface. The second thermal degradation (II) started from 180 °C and ended at 220 °C with a total mass loss of ~ 44.15% and in APTES treated nano-clay has a total mass of ~ 9.89%, which is attributed to the dehydroxylation of metal hydroxide and the removal of nitrate ions. The third thermal degradation (III) started from 220 °C and ended at 450 °C with a total mass loss of ~ 14.15% and in APTES treated nano-clay has a total mass of ~ 34.89%, which is attributed to the decomposition of the alkyl chain and the loss of OH. The mass loss peak corresponding to the absorbed water molecules was disappeared completely, indicating water consumption during the grafting of APTES with halloysite nano-clay. Further, the difference in weight loss corresponding to dehydroxylation was found to be narrowed as compared with unmodified halloysite clay and treated nano-clay. The reduced content of –OH groups confirmed their consumption during the condensation reaction with –Si–OH to form –Si–O–M.

3.3 SECM Studies

SECM images for the epoxy coated mild steel with and without silane modified halloysite nanoparticles in 3.5% NaCl with scratches at the tip potential of + 0.60 V (vs. Ag/AgCl/saturated KCl) are depicted in Figs. 3 and 4, respectively. The colour changes in the SECM images represent the local anodic and cathodic area in the scratched sample. SECM scans were done by rastering UME over the scratched coated surface by applying the tip potential of + 0.60 V. At this potential, the presence of ferrous ion can be detected through their oxidation to ferric ions [24]. The current measured at the scratch is significantly higher than that of other places. The tip current at the scratch of the epoxy coated mild steel increases with increase in days from 4.09 nA 1 day to 9.50 nA 40 days. This shows that the dissolution of Fe^{2+} increases with immersion days. The electrochemical behavior of epoxy APTES-modified halloysite coated mild steel is same as that of the epoxy coated mild steel. However, the tip current at the scratch

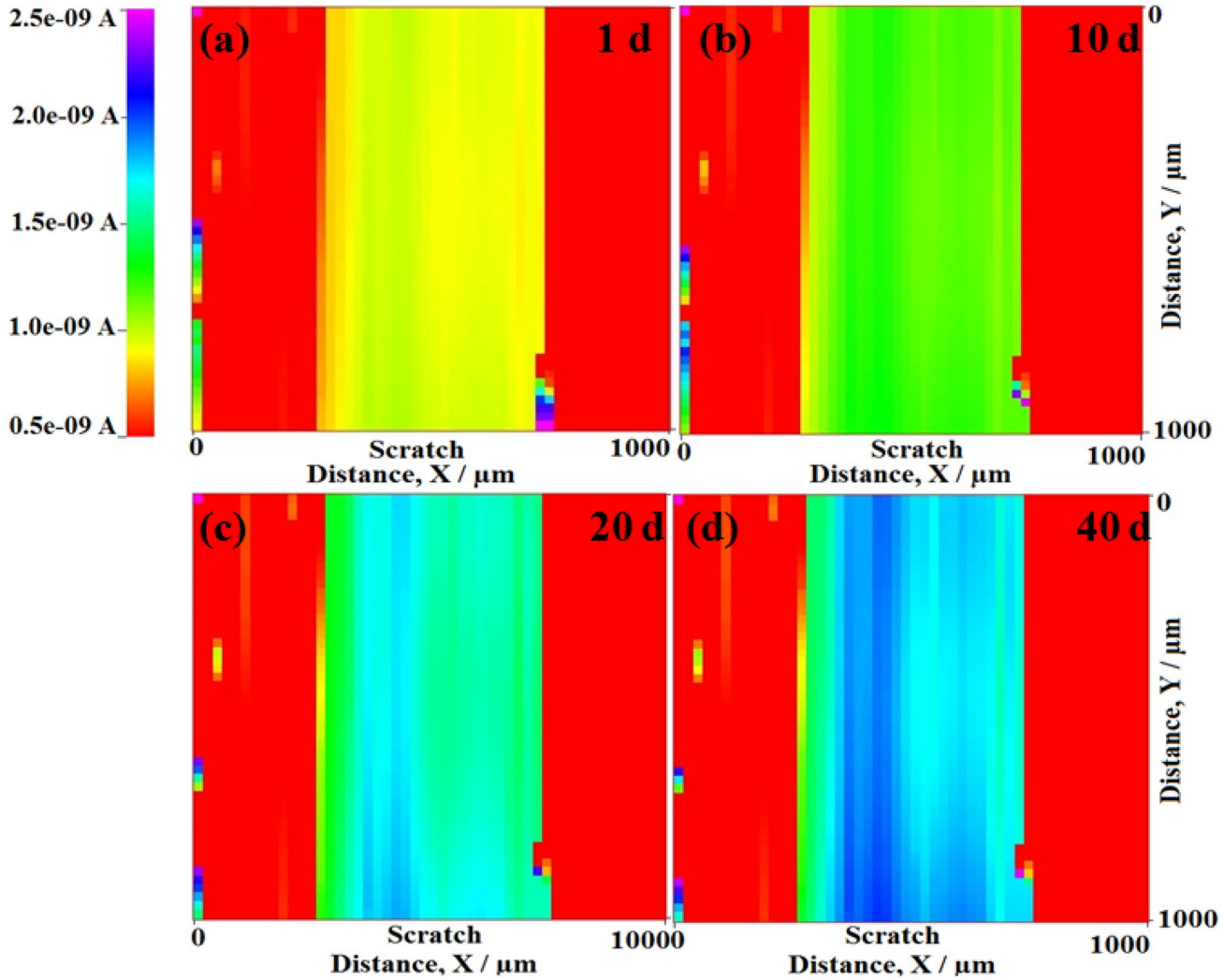

Fig. 3 SECM 2D images obtained for scratched epoxy-APTES/clay nanocomposite coated mild steel immersed in 3.5% NaCl solution for 1, 10, 20 and 40 days at tip potential + 0.60 V vs. Ag/AgCl/KCl reference electrode

increases very slowly as compared with the epoxy coated mild steel from 0.9 nA 1 day to 1.8 nA 40 days.

In the case of epoxy-APTES/clay nanocomposite coated mild steel, the tip current measured at the scratch is significantly smaller (1.8 nA) than that over the coated surface (9.5 nA). This behavior shows that the consumption of oxygen occurs at the scratch. As anodic dissolution of Fe^{2+} occurs, the concentration of oxygen is decreased by the consumption as cathodic reaction at the scratch. It is evident from the measurement that the presence of APTES-modified halloysite nanoparticles in the epoxy coating reduces the dissolution of iron from the metal surface by covering the surface by forming complexes. The formation of complexes on the metal surface provides additional barrier protection to the surface apart from the film resistance. Thus, the dissolution of Fe^{2+} at the scratch is reduced in epoxy-APTES/clay nanocomposite coated mild steel compared to epoxy coated mild steel.

3.4 Electrochemical Impedance Spectroscopy (EIS)

EIS measurements were performed for scratched samples in a 3.5% NaCl solution to evaluate the corrosion resistance of coated mild steel. Figure 5 Nyquist plots obtained for bare mild steel, pure epoxy and epoxy coated with different weight parameters of APTES functionalized clay nanoparticles immersed in 3.5% NaCl solution. Table 2 represents the fitted parameters of the EIS plots of the epoxy coating with different weight percentage of APTES/clay nanoparticles at 1 day immersion in 3.5% NaCl solution. It is observed from Table 2 that the maximum resistance is observed for epoxy coating with 4 wt% of APTES functionalized clay nanoparticles. The addition of APTES/clay nanoparticle up to

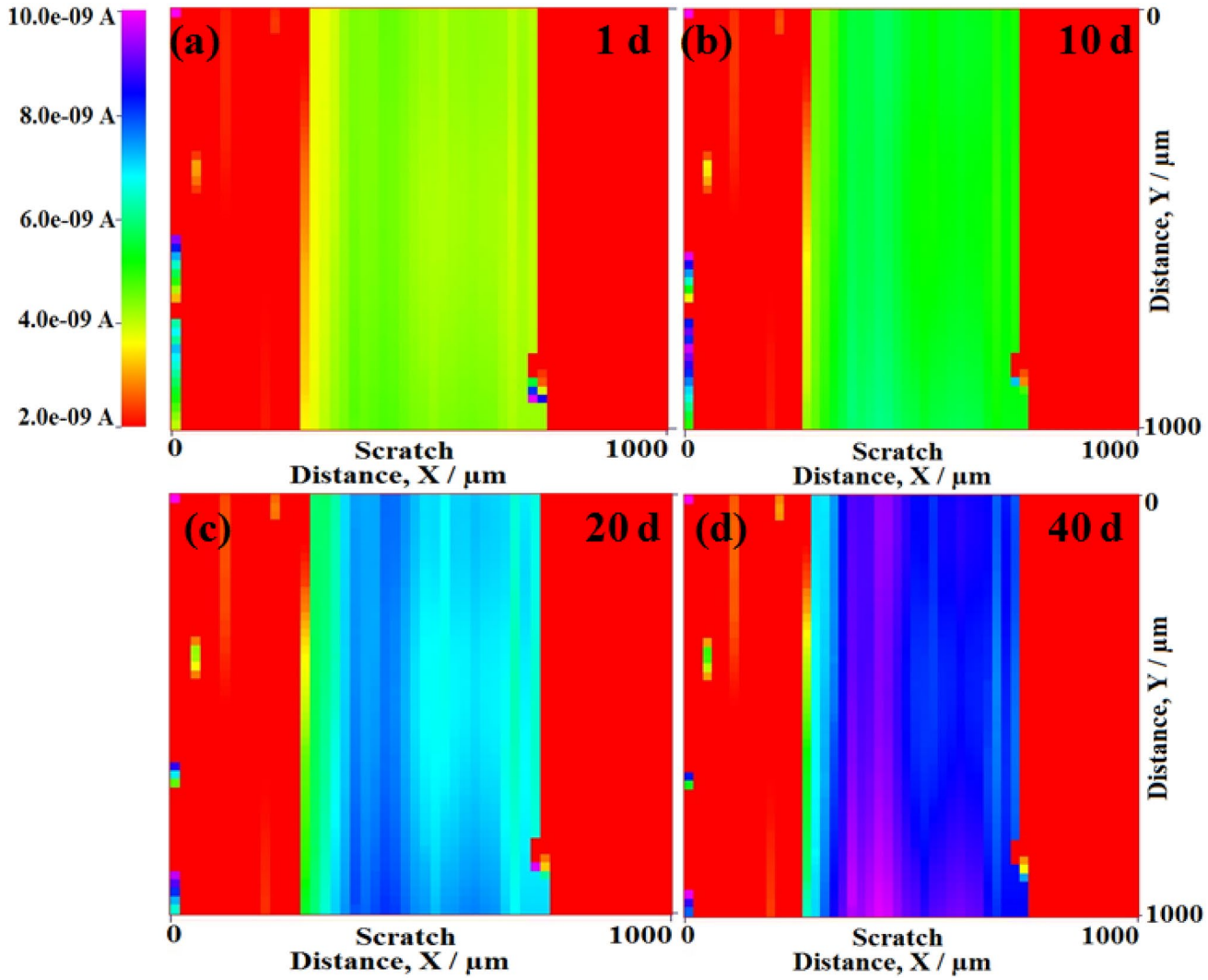

Fig. 4 SECM 2D images obtained scratched pure epoxy coated mild steel immersed in 3.5% NaCl solution for 1, 10, 20 and 40 days at tip potential + 0.60 V vs. Ag/AgCl/KCl reference electrode

4 wt% to the epoxy coating increased the values of coating and charge transfer resistances. With increasing the weight percentage beyond 4 wt% (i.e.; 5 wt%) of APTES functionalized clay nanoparticles, the resistance has been reduced due to the agglomeration of the APTES/clay nanoparticles, which showed higher density and reduced uniformity of the coatings. Thus, the optimal weight percentage of APTES functionalized clay nanoparticles were considered as 4. Figures 6 and 7 presents Bode plots obtained for epoxy-APTES/clay nanocomposite coated steel and pure epoxy coated mild steel respectively immersed in 3.5% NaCl solution for 1 day, 10 days, 20 days and 40 days. The corresponding typical Nyquist plots are shown in Fig. 8 for both epoxy-APTES/clay nanocomposite coated steel and pure epoxy substrate. It was possible to fit all the impedance spectra using the equivalent circuit model shown in Fig. 9. Table 3 displays the fitted data of derived charge transfer resistance (R_{ct}) and double layer capacitance (CPE_{dl}) values. The Rct value decreased from 129,532 to 72,143 Ω cm^2 and CPE_{dl} increased from 8.125×10^{-5} to 6.984×10^{-2} with increased immersion days for epoxy coated mild steel, whereas R_{ct} value decreased from 238,967 to 170,462 Ω cm^2 and CPE_{dl} value increased from 3.994×10^{-11} to 8.785×10^{-5} with increased immersion days. It was obvious that the R_f and R_{ct} decreased with the immersion time. This indicated that the passive film coating on the surface of the steel was acting as the protecting layer, while the chloride content was below the threshold value. However, the passive film became unstable and exhibited local breakdown when the immersion time increased. Meanwhile, the pitting pores took place in some positions of the steel surface. Consequently, R_f value (249,956 Ω cm^2 for 1 day immersion 135,946 Ω cm^2 for

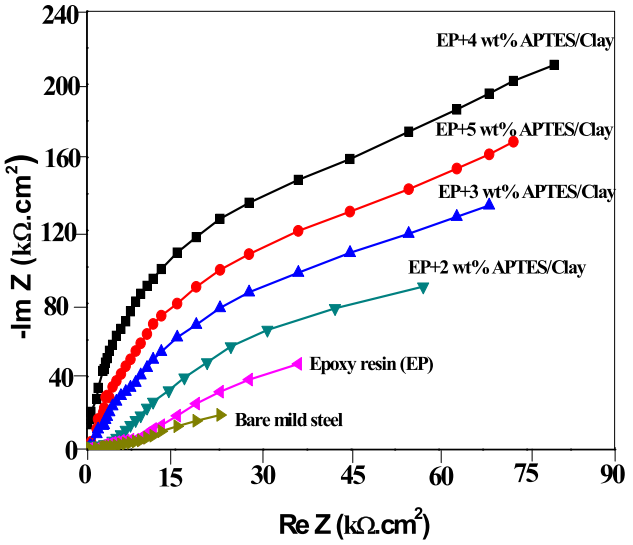

Fig. 5 Nyquist plots obtained for bare mild steel, pure epoxy and epoxy coated with different weight percentage of APTES functionalized clay nanoparticles immersed in 3.5% NaCl solution

40 days immersion) decreased when the immersion time increased. It indicated that the capacitances increased with the immersion time and raised remarkably when the immersion time increased to 40 days. The R_f is actually thought to demonstrate ionic transport through the coating film. Thus, the decrease of R_f during the first few days of the test is attributed to the penetration of the solution through the coating. The decrease of R_f during the test time indicates a loss of the barrier properties of the film. An increase of the modified clay beyond 4 wt% in the coating decreased the barrier properties and did not improve corrosion protection due to the agglomeration.

3.5 Polarization Studies

Figure 10 shows the polarization curves for both epoxy-APTES/clay nanocomposite and epoxy coated mild steel in 3.5% NaCl solution for different immersion times. The anodic and cathodic curves were extrapolated to the corrosion potential to find the corrosion current densities. The values of corrosion potential (E_{corr}) and corrosion current density (I_{corr}) are presented in Table 4. The results show that by increasing the immersion time, the values of polarization resistance decrease considerably. The I_{corr} value of both epoxy and epoxy-APTES/clay nanocomposite coated steel increased with immersion time. However, I_{corr} value of epoxy coated steel is significantly higher 2.94 μA/cm^2 at 40 days of immersion (destabilizing the passive film, which results in a higher rate of corrosion) compared to epoxy-APTES/clay nanocomposite coated steel 1.63 μA/cm^2 at 40 days of immersion (indicating the stability of the passive film formed on the surface). The R_p value of both epoxy and epoxy-APTES/clay nanocomposite coated steel decreased with immersion time. Similarly, a significant decrease in R_p value is noticed for epoxy coated steel (2.68 kΩ cm^2 at 40 days of immersion) compared to epoxy-APTES/clay nanocomposite coated steel (5.25 kΩ cm^2 at 40 days of immersion). Extremely high corrosion resistance is obtained for the epoxy/APTES coated mild steel. Therefore, it can be concluded that epoxy-APTES/clay nanocomposite coated steel exhibits an excellent corrosion inhibition performance than pure epoxy coated steel.

3.6 FE-SEM/EDX Analysis

Figure 11 shows the FE-SEM micrograph of epoxy-APTES/clay nanocomposite coated steel for 1 day and 40 days immersed in 3.5% NaCl solution. The SEM micrograph revealed the tubular shaped morphology for 1 day immersed sample. The coating surfaces were smooth, but the relatively randomly oriented nanoparticles were clearly detectable in them. However, micro pores are visible on the surface of the epoxy-APTES/clay nanocomposite coated steel at 40 days immersion in chloride medium. This enhances the initiation of corrosion process at the metal/coating interface.

The EDX elemental analysis of epoxy-APTES/clay nanocomposite coated steel for 1 day and 40 days immersed in 3.5% NaCl solution shows the peaks of carbon, oxygen, nitrogen, and silicon which indicates the presence of halloysite and APTES molecules in copolymer chain. Besides, they show that halloysite clay was successfully modified with APTES. Silane grafting can be confirmed by the

Table 2 The fitted parameters of the EIS plots of the epoxy coating with different weight percentage of APTES/clay nanoparticles at 1 day immersion in 3.5% NaCl solution

Wt% of APTES/clay in epoxy coating	R_s Ω cm^2	R_f Ω cm^2	CPE_f (F cm^{-2} s^n)	R_{ct} Ω cm^2	CPE_{dl} (F cm^{-2} s^n)	$\|Z\|$ Ω cm^2	n_{coat}
0	28.3	76,345	3.986×10^{-5}	129,532	8.125×10^{-5}	104,865	0.78
1	26.2	98,785	9.989×10^{-6}	151,940	9.579×10^{-6}	119,973	0.80
2	24.0	139,568	4.658×10^{-6}	172,845	8.642×10^{-7}	144,019	0.82
3	19.1	180,320	5.957×10^{-7}	195,842	1.895×10^{-8}	172,847	0.84
4	10.4	249,956	8.275×10^{-11}	238,967	3.994×10^{-11}	213,985	0.88
5	15.9	211,644	7.655×10^{-9}	218,989	6.378×10^{-9}	191,141	0.86

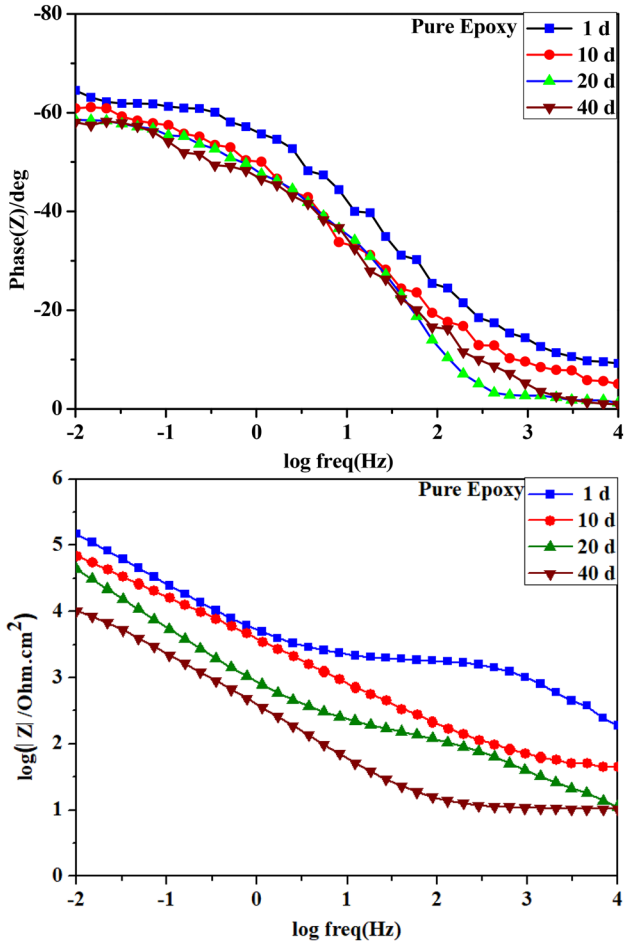

Fig. 6 Bode plots obtained for pure epoxy coated mild steel immersed in 3.5% NaCl solution for 1, 10, 20 and 40 days

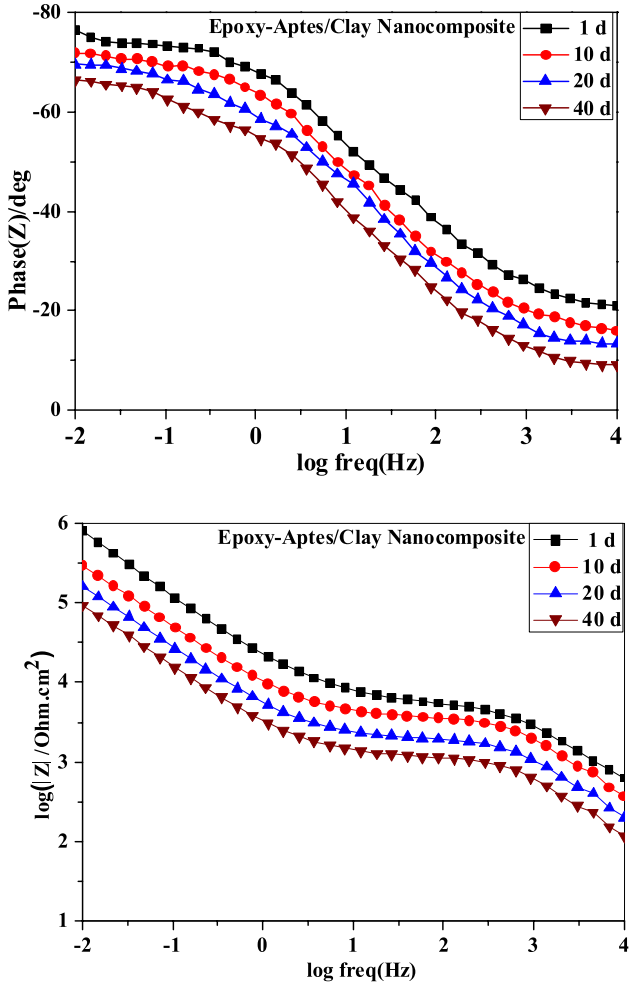

Fig. 7 Bode plots obtained for epoxy-APTES/clay nanocomposite coated mild steel immersed in 3.5% NaCl solution for 1, 10, 20 and 40 days

presence of nitrogen content. The quantity of amino groups in the APTES-modified halloysite clay depends on the type of functionality of amino groups in the silane coupling agent, due to the presence of hydroxyl groups on the APTES-modified halloysite clay which results in more hydrogen bond interactions between the modified halloysite clay [28]. Thus, modified clay with APTES is more effective in improving the mechanical properties. These observations corroborate the results obtained from FTIR and FE-SEM analyses.

3.7 XRD Analysis

Figure 12 shows the XRD pattern for the epoxy-APTES/clay nanocomposite immersed in 3.5% NaCl for 1 day and 40 days, respectively. XRD analysis for 1 day and 40 days immersion of epoxy-APTES/clay nanocomposite showed formation of corrosion products on the metal surface. The corrosion products of the upper surface were α-FeOOH and beneath the surface were mainly due to γ-FeOOH. However, on prolonged immersion in NaCl, γ-FeOOH could be converted to Fe_3O_4. This indicates that complete corrosion takes place on the metal surface. It is also observed that the intensity of these iron peaks (γ-FeOOH) is raised in 40 days immersion. These findings confirm that there is a corrosion formation both in 1 day and 40 days immersion, but higher corrosion product formation in 40 days compared to 1 day immersion leads to the slowing down of the corrosion process. In 40 days, we could see the enhanced peaks obtained for γ-FeOOH and small peak obtained for Fe_3O_4, which reveal that the corrosion process occurs with controlled process along with the epoxy-APTES/clay nanocomposite coatings on mild steel.

3.8 Mechanical Properties

3.8.1 Microhardness

Figure 13 shows the graphical representation of hardness test value before and after immersion for different days in 3.5%

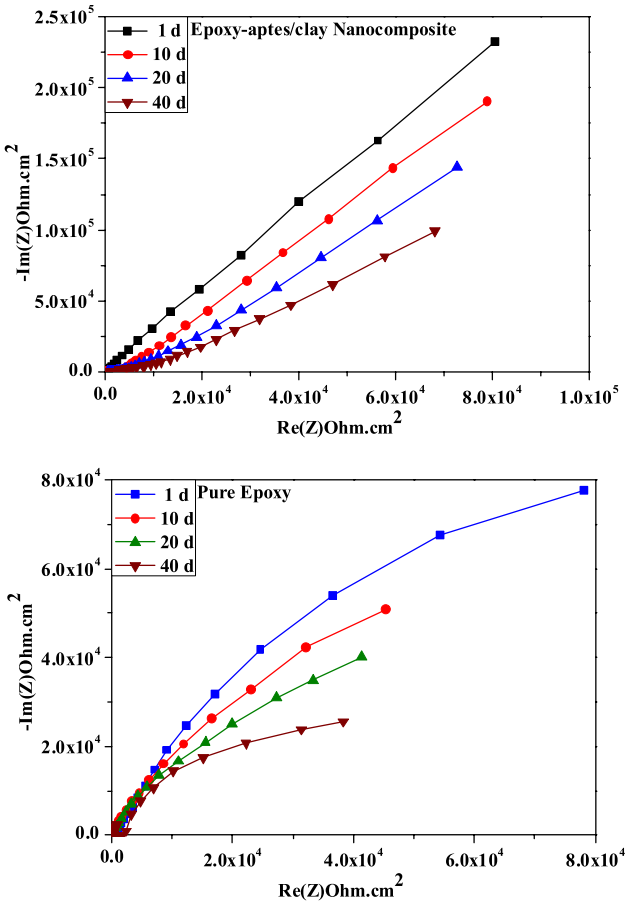

Fig. 8 Nyquist plots obtained for epoxy-APTES/clay nanocomposite and pure epoxy coated mild steel immersed in 3.5% NaCl solution for 1, 10, 20 and 40 days

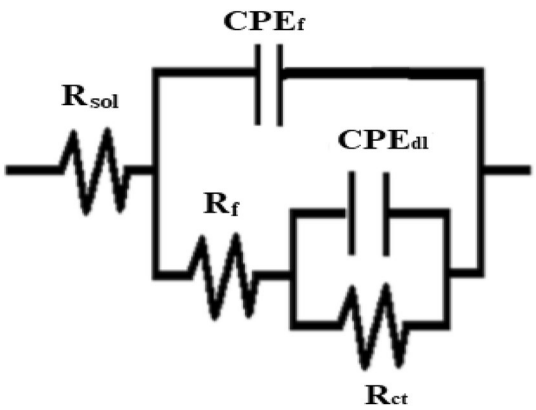

Fig. 9 Equivalent circuit model for both epoxy-APTES/clay nanocomposite and pure epoxy coated mild steel in 3.5% NaCl solution at different days of immersion

NaCl solution. The hardness tests performed for pure epoxy and epoxy-APTES/clay nanocomposite for 1 day, 10 days, 20 days, and 40 days. The values of hardness test were lower in the pure epoxy and higher in the epoxy-APTES/clay for each day. The high hardness value of 610 MPa was obtained for epoxy-APTES/clay nanocomposite coated sample, whereas the lowest value of 90 MPa was obtained for epoxy coated steel after 40 days of immersion. The higher coating hardness strength for epoxy-APTES/clay nanocomposite coated sample shows lower porosity. In general, the highest hardness values were found before immersion and the lowest is obtained after immersion.

3.8.2 Pull Off Adhesion Test

Figure 14a represents the adhesion test values before and after immersion for different days in 3.5% NaCl solution. Epoxy-APTES/clay nanocomposite had a very good adhesion to mild steel substrates, compare to pure epoxy. The adhesion strength of pure epoxy composite is 5.5 MPa before immersion, and 2.5 MPa for 40 days immersion and it was increased up to 8.5 MPa before immersion and 6.0 MPa for 40 days immersion in epoxy-APTES/clay nanocomposite. These results show that all the samples have an excellent adhesion before their exposure to the electrolyte. There was no increase in adhesion strength between coating and the metal substrate, but there was a significant reduction in the adhesion strength. It may be due to the hydrophilic properties of nano fillers that cause the gathered water under coating and decreasing the coating adhesion to the metal surface.

3.8.3 Tensile Test

Figure 14b shows the results of tensile strength test for prepared samples for different days of exposure in the 3.5% NaCl solution. It is obvious that the ultimate tensile strength increased with decreased immersion time, but pure epoxy coated sample at 40 days had relatively lower tensile strength of 30 MPa than the epoxy-APTES/clay nanocomposite (70 MPa) at 40 days because of elasticity. Epoxy APTES/clay nanocomposite has ultimate tensile strength and it can withstand strain, torsion and bending without breaking the strength approximately 70 MPa.

4 Conclusion

This work described an effective approach to improve corrosion resistance of an epoxy-based coating by employing APTES-treated clay nanoparticles. The clay nanoparticles were successfully modified using a silane coupling agent (APTES) which was confirmed by FTIR, and TGA analysis. The APTES coupling agent was employed to improve the dispersing of clay nanoparticles in epoxy coatings and increasing the possible chemical interactions of APTES

Table 3 The fitted parameters of the EIS plots of epoxy-APTES/clay nanocomposite and pure epoxy coated steel in 3.5% NaCl solution

Coating	Immersion (day)	R_s Ω cm^2	R_f Ω cm^2	CPE_f (F cm^{-2} s^n)	R_{ct} Ω cm^2	CPE_{dl} (F cm^{-2} s^n)	$\|Z\|$ Ω cm^2	n_{coat}
Epoxy	1	28.3	76,345	3.986×10^{-5}	129,532	8.125×10^{-5}	104,865	0.78
	10	30.1	71,934	5.994×10^{-4}	112,583	9.321×10^{-4}	68,984	0.76
	20	31.1	56,753	8.436×10^{-3}	95,225	11.125×10^{-3}	39,983	0.73
	40	33.5	39,724	4.296×10^{-2}	72,143	6.984×10^{-2}	33,756	0.70
Epoxy-APTES/clay	1	10.4	249,956	8.275×10^{-11}	238,967	3.994×10^{-11}	213,985	0.88
	10	15.6	210,832	7.369×10^{-9}	219,368	6.485×10^{-8}	149,635	0.86
	20	19.3	171,341	5.584×10^{-7}	192,985	1.998×10^{-8}	122,764	0.82
	40	24.7	135,946	4.475×10^{-6}	170,462	8.785×10^{-5}	85,934	0.78

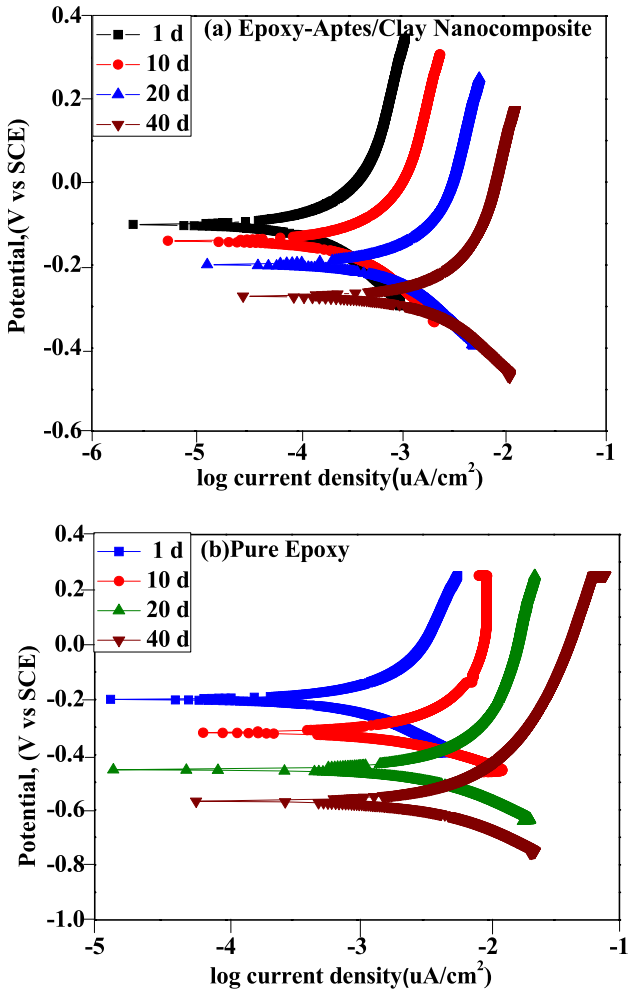

Fig. 10 Polarization curves of **a** epoxy-APTES/clay nanocomposite **b** pure epoxy coated mild steel immersed in 3.5% NaCl solution for 1, 10, 20 and 40 days

Table 4 Fitted parameters of polarization cures for epoxy-APTES/clay nanocomposite and pure epoxy coated steel in 3.5% NaCl solution

Coating	Immersion time (day)	E_{Corr} (mv) Vs. SCE	I_{Corr} (μA/cm^2)	R_p (kΩ cm^2)
Epoxy	1	− 348	1.25	6.94
	10	− 427	1.99	5.98
	20	− 498	2.25	4.75
	40	− 746	2.94	2.68
Epoxy-APTES/clay	1	− 229	0.58	8.91
	10	− 342	1.12	7.42
	20	− 475	1.48	6.46
	40	− 624	1.63	5.25

functional groups on clay nanoparticle and epoxy matrix. By incorporation of APTES/clay nanoparticles, the corrosion rate was reduced significantly. The results from EIS, polarization and SECM techniques revealed that 4 wt% APTES/clay nanoparticles considerably improved the corrosion resistance of epoxy coating via increasing barrier properties, which reduced corrosive ion movement and decreased the corrosion rate. Morphological studies of the epoxy-APTES/clay nanocomposites using FE-SEM revealed good dispersion of nanofillers into an epoxy coated sample which lead to improving the mechanical and barrier properties. The values of adhesion and tensile strengths increased significantly for epoxy-APTES/clay nanocomposite coated steel. The microhardness test value increased for epoxy-APTES/clay nanocomposite coated steel as compared to pure epoxy coated sample.

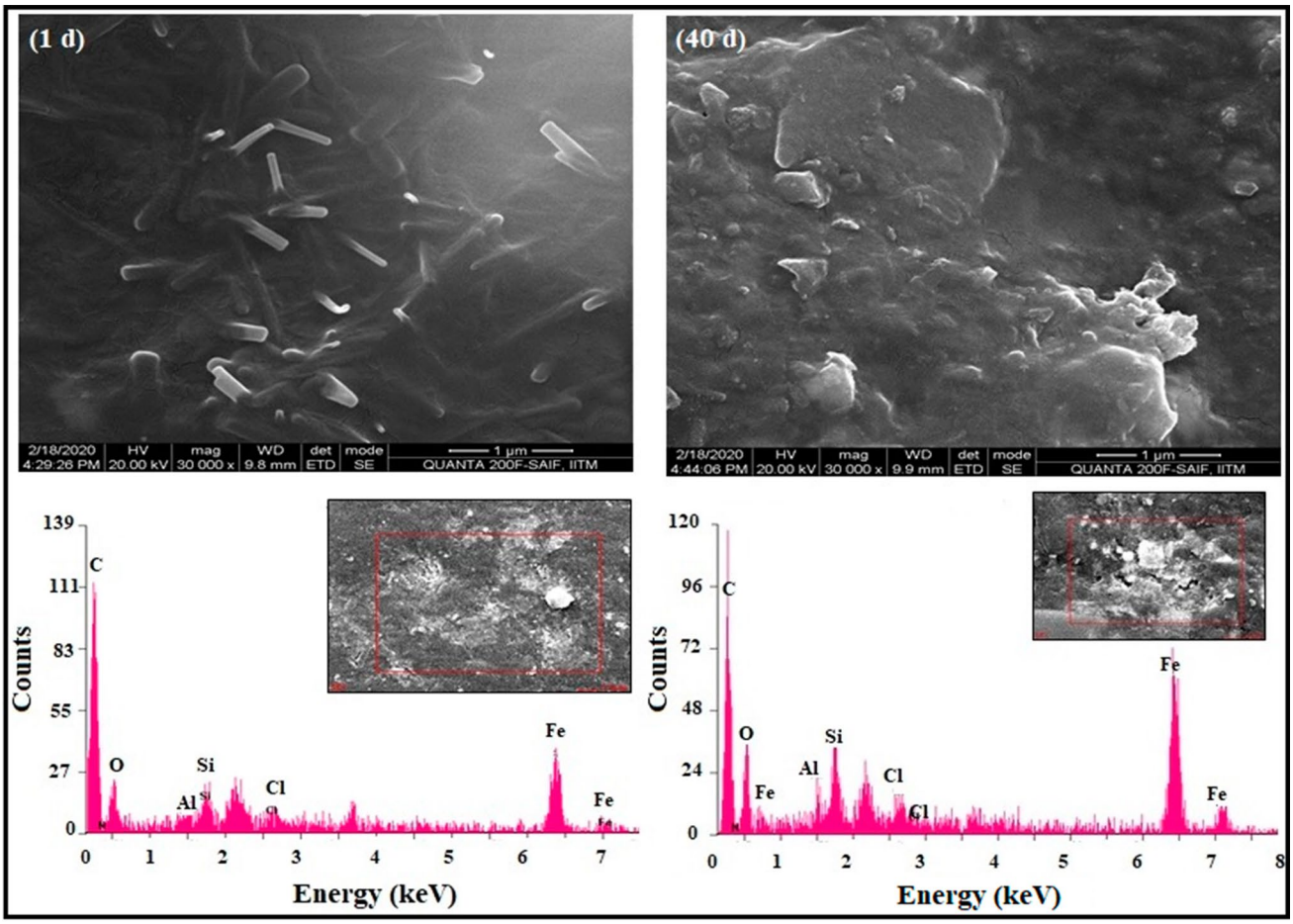

Fig. 11 SEM and EDX images of epoxy-APTES/clay nanocomposite for 1 day and 40 days immersed in 3.5% NaCl solution

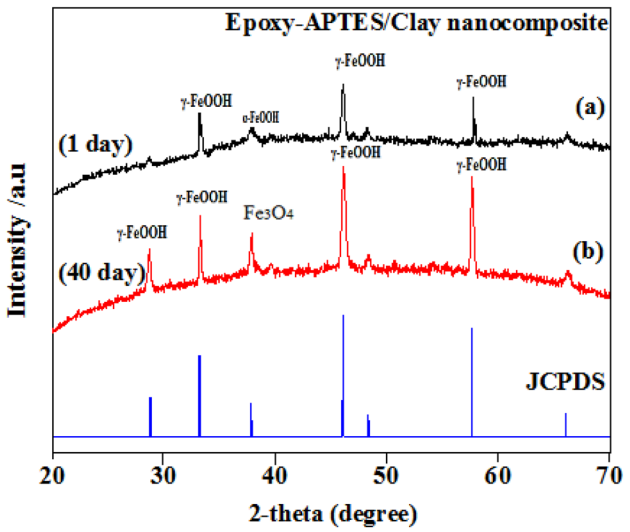

Fig. 12 XRD images of epoxy-APTES/clay nanocomposite for 1 day and 40 days immersed in 3.5% NaCl solution

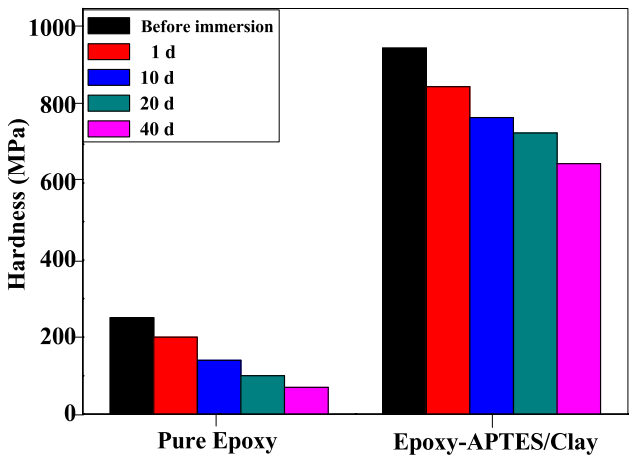

Fig. 13 Bar graph of hardness of epoxy-APTES/clay nanocomposite and pure epoxy coated mild steel compared for before immersion and after immersion in 3.5% NaCl solution for 1, 10, 20 and 40 days

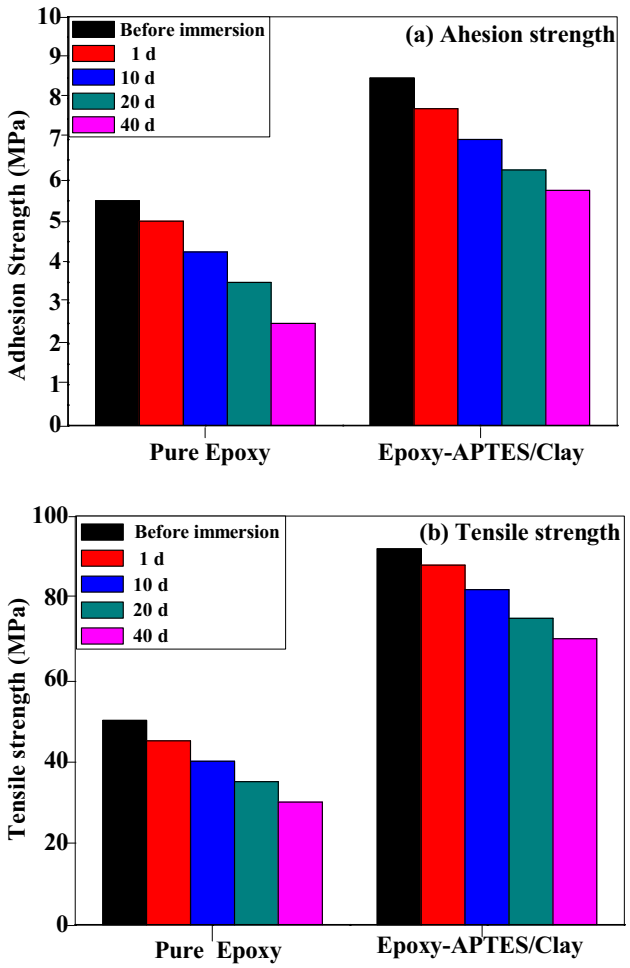

Fig. 14 Bar diagram of **a** adhesion and **b** tensile strength of epoxy-APTES/clay nanocomposite and pure epoxy coated mild steel compared for before immersion and after immersion in 3.5% NaCl solution for 1, 10, 20 and 40 days

Compliance with Ethical Standards

Conflict of interest The authors declare that they have no conflict of interest.

References

1. Pal P, Kundu MK, Malas A, Das CK (2013) Compatibilizing effect of halloysite nanotubes in polar–nonpolar hybrid system. Appl Polym Sci 131:39587
2. Li Z, Expósito DF, Gonzalez AJ, Wang DY (2017) Natural halloysite nanotube based functionalized nano hybrid assembled via phosphorus-containing slow release method: a highly efficient way to impart flame retardancy to polylactide. Eur Polym J 93:458–470
3. Kryuchkova M, Danilushkina A, Lvov Y, Fakhrullin R (2016) Evaluation of toxicity of nanoclays and graphene oxide in vivo: a *Paramecium caudatum* study. Environ Sci Nano 3:442–452
4. Vahedi V, Pasbakhsh P (2014) Instrumented impact properties and fracture behaviour of epoxy/modified halloysite nanocomposites. Polym Test 39:101–114
5. Peprnicek T, Duchet J, Kovarova L, Malac J, Gerard JF, Simonik J (2006) Poly (vinyl chloride)/clay nanocomposites: x-ray diffraction, thermal and rheological behavior. Polym Degrad Stab 91:1855–1860
6. Lee JY, Lee HK (2004) Characterization of organo bentonite used for polymer nanocomposites. Mater Chem Phys 85:410–415
7. Morawiec J, Pawlak A, Slouf M, Galeski A, Piorkowska E, Krasnikowa N (2005) Preparation and properties of compatibilized LDPE/organo-modified montmorillonite nanocomposites. Eur Polym J 41:1115–1122
8. Gorrasi G, Tortora M, Vittoria V (2003) Vapor barrier properties of polycaprolactone montmorillonite nanocomposites: effect of clay dispersion. Polymer 44:2271–2279
9. Someya Y, Shibata M (2005) Morphology, thermal, and visco elastic properties of poly(glycidyl methacrylate-co-methyl methacrylate)-based nanocomposites with various organo modified clays. Polymer 46:4891–4898
10. Park J, Jana SC (2004) Adverse effects of thermal dissociation of alkyl ammonium ions on nanoclay exfoliation in epoxy–clay systems. Polymer 45:7673–7679
11. Cao X, James Lee L, Widya MTC (2005) Polyurethane/clay nanocomposites foams: processing, structure and properties. Polymer 46:775–783
12. Raj XJ (2017) Application of EIS and SECM studies for investigation of anticorrosion properties of epoxy coatings containing zinc oxide nanoparticles on mild steel in 3.5% NaCl solution. J Mater Eng Perform 26(7):3245–3253
13. Raj XJ, Nishimura T (2014) Corrosion protection performance of epoxy coated high tensile strength steel measured by scanning electrochemical microscope and electrochemical impedance spectroscopy techniques. ISIJ Int 54(3):693–699
14. Yeh JM, Chen CL, Chen YC (2002) Enhancement of corrosion protection effect of poly(*o*-ethoxyaniline) via the formation of poly(*o*-ethoxyaniline)-clay nanocomposite materials. Polymer 43:2729–2746
15. Hang TTX, Truc TA, Nam TH, Oanh VK, Jorcin JB, Pebere N (2007) Corrosion protection of carbon steel by an epoxy resin containing organically modified clay. Surf Coat Technol 201:7408–7415
16. Sugama T (2006) Polyphenylene sulfied/montomorillonite clay nanocomposite coatings: their efficacy in protecting steel against corrosion. Mater Lett 60:2700–2706
17. Yeh JM, Huang HY, Chen CL, Su WF, Yu YH (2006) Siloxane-modified epoxy resin-clay nanocomposite coatings with advanced anticorrosive properties prepared by a solution dispersion approach. Surf Coat Technol 200:2753–2763
18. Hedenqvist MS, Backman A, Gallstedt M, Boyd RH, Gedde UW (2006) Morphology and diffusion properties of whey/montmorillonite nanocomposites. Compos Sci Technol 66:2350–2359
19. Hackman I, Hollaway L (2006) Epoxy-layered silicate nanocomposites in civil engineering. Compos A 37:1161–1170
20. Azeez AA, Rhee KY, Park SJ, Hui D (2013) Epoxy clay nanocomposites—processing, properties and applications: a review. Compos B Eng 45:308–320
21. Boomadevi Janaki G, Xavier JR (2020) Evaluation of mechanical properties and corrosion protection performance of surface modified nano-alumina encapsulated epoxy coated mild steel. J Bio Tribo Corros 6:20. https://doi.org/10.1007/s40735-019-0316-7
22. Tomic MD, Dunjic B, Likic V, Bajat J, Rogan J, Djonlagic J (2014) The use of nanoclay in preparation of epoxy anticorrosive coatings. Prog Org Coat 77:518–527

23. Xavier JR (2018) Investigation on the effect of nano-ceria on the epoxy coatings for corrosion protection of mild steel in natural seawater. Anti-Corros Methods Mater 65:38–45
24. Xavier JR, Nallaiyan R (2016) Application of EIS and SECM studies for investigation of anticorrosion properties of epoxy coatings containing ZrO_2 nanoparticles on mild steel in 3.5% NaCl solution. J Fail Anal Prev 16:1082–1091
25. Joseph Raj X, Nishimura T (2016) Evaluation of the corrosion protection performance of epoxy-coated high manganese steel by SECM and EIS techniques. J Fail Anal Prev 16:417–426
26. ASTM G106 (2004) Standard practice for verification of algorithm and equipment for electrochemical impedance measurements. ASTM International, West Conshohocken, PA, USA
27. Xavier JR, Nishimura T (2017) Evaluation of the corrosion protection performance of epoxy coatings containing Mg nanoparticle on carbon steel in 0.1 M NaCl solution by SECM and EIS techniques. J Coat Technol Res 14:395–406. https://doi.org/10.1007/s11998-016-9856-7
28. Yuan P, Southon PD, Hook JM (2008) Functionalization of halloysite clay nanotubes by grafting with aminopropyltriethoxysilane. J Phys Chem C 112:15742–15751